NASA TN D-468

TECHNICAL NOTE

D-468

DISTRIBUTION OF TIME-AVERAGED PRESSURE FLUCTUATIONS ALONG THE BOUNDARY OF A ROUND SUBSONIC JET

By Walton L. Howes

Lewis Research Center
Cleveland, Ohio

NATIONAL AERONAUTICS AND SPACE ADMINISTRATION

WASHINGTON October 1960

NATIONAL AERONAUTICS AND SPACE ADMINISTRATION

TECHNICAL NOTE D-468

DISTRIBUTION OF TIME-AVERAGED PRESSURE FLUCTUATIONS ALONG THE BOUNDARY OF A ROUND SUBSONIC JET

By Walton L. Howes

SUMMARY

A semiempirical analysis of the equation for incompressible fluctuations in a turbulent fluid, using similarity relations for round subsonic jets with uniform exit velocity, is used to predict the shape of the time-averaged fluctuation-pressure distribution along the mean-velocity boundary of jets. The predicted distribution is independent of distance downstream of the nozzle exit along the mixing region, inversely proportional to the distance downstream along the region of mean-velocity self-preservation, and proportional to the inverse square of the distance downstream along the fully developed region.

Experimental results were in fair agreement with the theory. However, the measured fluctuation-pressure distributions were found to be very sensitive to changes in jet temperature and jet-nozzle profile, especially near the nozzle. These factors are not included in the theory. Increased jet temperatures produce increased pressure fluctuations and violation of similarity conditions. Nozzle-profile modifications may lead to violation of the uniform-exit-velocity requirement imposed in the theory.

INTRODUCTION

Some previous theoretical studies of noise from round subsonic jets (refs. 1 to 3) have related the radiated acoustic power to the strength distribution of noise sources along a jet. Measurements to confirm the theories have not been performed. On the other hand, measurements of pressure fluctuations along the mean-velocity boundary of a jet have been performed (ref. 4); but no attempt has been made to predict theoretically the shape of the fluctuation-pressure distribution. This latter problem appears to be as important as the former in evaluating the noise characteristics of jets and is considered herein. The previous theoretical studies in references 3 and 5 are particularly relevant to the following discussion.

The author is greatly indebted to Professor Herbert S. Ribner for suggesting the possibility of a mathematical attack on the present problem and for his many enlightening discussions of jet noise theory.

THEORY

Consider a continuous, perfect, homogeneous, inviscid medium containing a region of turbulence possessing a mean motion, but free of sources of matter and external forces. The appropriate exact equation for fluctuations which occur within the medium is, in rectangular Cartesian coordinates, $x_i (i = 1, 2, 3)$,

$$\frac{\partial^2 p}{\partial x_i^2} - \frac{\partial^2 \rho}{\partial t^2} = - \frac{\partial^2}{\partial x_i \partial x_j} (\rho v_i v_j) \tag{1}$$

where p is pressure, ρ is density, v_i are velocity components, and t is time. (All symbols are defined in the appendix.)

A pressure-sensitive microphone placed along the mean-velocity boundary of a jet will respond to temporal fluctuations of the pressure associated with incompressibility, as well as to temporal fluctuations of the pressure associated with compressibility. The former fluctuations, called "pseudosound," are not radiated, whereas the latter fluctuations (sound) are propagated acoustically. Because the pressure fluctuations very near the jet are dominantly associated with incompressibility (refs. 1 and 6), the detected fluctuations should be described essentially by the incompressible part of the inhomogeneous wave equation (1), namely

$$\frac{\partial^2 p}{\partial x_i^2} = -\rho_0 \frac{\partial^2}{\partial x_i \partial x_j} (v_i v_j) \tag{2a}$$

where the density ρ_0 is constant over space and time. Set $p = \overline{p} + \tilde{p}$ and $v_k = \overline{v}_k + \tilde{v}_k$, where $\overline{p}$ and $\overline{v}_k$ are temporal-mean values and $\tilde{p}$ and $\tilde{v}_k$ are fluctuations associated with incompressibility. (The fluctuations $\tilde{p}$ and $\tilde{v}_k$ correspond, respectively, to pseudosound and turbulence.) From the resulting equation, subtract its temporal mean. The result is

$$\frac{\partial^2 \tilde{p}}{\partial x_i^2} = -\rho_0 \frac{\partial^2 \psi_{ij}}{\partial x_i \partial x_j} \tag{2b}$$

where

$$\psi_{ij} = 2\overline{v}_i\tilde{v}_j + \tilde{v}_i\tilde{v}_j - \overline{\tilde{v}_i\tilde{v}_j} \tag{3}$$

Equations (2) possess the form of Poisson's equation. Hence, the solution of equation (2b) is

$$\tilde{p}(\vec{x};\ t) = -\frac{\rho_0}{4\pi}\int \frac{\partial^2\psi_{ij}}{\partial y_i \partial y_j}\,\frac{d^3\vec{y}}{|\vec{y} - \vec{x}|} \tag{4}$$

where $\vec{x}$ denotes the observation point, as shown in figure 1, $\vec{y}$ denotes source points, the volume integration is over all space (but for practical purposes, only over the source region), and the velocity components are functions of $\vec{y}$ and t. By performing a double partial integration, equation (4) becomes (ref. 7)

$$\tilde{p}(\vec{x};t) = -\frac{\rho_0}{4\pi}\int \psi_{ij}(\vec{y};t)\,\frac{(y_i - x_i)(y_j - x_j)}{|\vec{y} - \vec{x}|^5}\,d^3\vec{y} \tag{5}$$

Equation (5) expresses the instantaneous pressure fluctuation at one observation point (x_1,x_2,x_3) as a function of simultaneous instantaneous velocity distributions throughout the turbulent region. However, in order to associate $\tilde{p}$ with measurable velocity distributions, the velocities, hence $\tilde{p}$, must be expressed in the form of time averages. The time average of $\tilde{p}$ is zero, but, in general, the space-time covariance of $\tilde{p}$ is not zero if the spatial separation, or time delay, or both, are not excessively large. Thus, consider

$$\overline{\tilde{p}(\vec{x};t)\tilde{p}(\vec{x}';\ t')}$$

$$= \frac{\rho_0^2}{16\pi^2}\overline{\int \psi_{ij}(\vec{y};t)\,\frac{(y_i - x_i)(y_j - x_j)}{|\vec{y} - \vec{x}|^5}\,d^3\vec{y}\int \psi_{kl}(\vec{y}';t')\,\frac{(y'_k - x'_k)(y'_l - x'_l)}{|\vec{y}' - \vec{x}'|^5}\,d^3\vec{y}'}$$

The vectors $\vec{x},\vec{x}'$ denote different observation points; $\vec{y},\vec{y}'$ denote different source points; and t,t' denote different times. In the present instance interest is confined to the mean-square-pressure fluctuation. Hence, $\vec{x}' \equiv \vec{x}$, and $t' \equiv t$. Consequently,

$$\overline{\tilde{p}^2(\vec{x};\ t)}$$

$$= \frac{\rho_0^2}{16\pi^2}\iint \overline{\psi_{ij}(\vec{y};t)\psi_{kl}(\vec{y}';t)}\,\frac{(y_i - x_i)(y_j - x_j)}{|\vec{y} - \vec{x}|^5}\,\frac{(y'_k - x_k)(y'_l - x_l)}{|\vec{y}' - \vec{x}|^5}\,d^3\vec{y}\,d^3\vec{y}' \tag{6}$$

where $\overline{\psi_{ij}(\vec{y};t)\psi_{kl}(\vec{y}';t)}$ represents a space covariance. Usually the space covariance of a quantity is expressed as a function of location in space and the separation of the observation points (source points in the present instance). Thus, consider the transformation

$$\vec{y} \equiv \vec{y}$$

$$\vec{y}' = \vec{y} + \vec{z}$$

where $\vec{z}$ connects source points (see fig. 1). Then, equation (6) becomes

$$\overline{\tilde{p}^2(\vec{x};t)} = \frac{\rho_0^2}{16\pi^2} \iint \overline{\psi_{ij}(\vec{y};t)\psi_{kl}(\vec{y}+\vec{z};t)} \frac{(y_i - x_i)(y_j - x_j)}{|\vec{y} - \vec{x}|^5} \frac{(y_k + z_k - x_k)(y_l + z_l - x_l)}{|\vec{y} + \vec{z} - \vec{x}|^5} \, d^3\vec{y} \, d^3\vec{z} \tag{7}$$

The integrations indicated in equation (7) appear considerably more complex than those performed in reference 5 because any product $\overline{\psi_{ij}(\vec{y};t)\psi_{kl}(\vec{y}';t)}$ is a function of $\vec{y}$ and $\vec{z}$, rather than $\vec{z}$ alone. Performing the integration does not appear presently feasible. This prevents the computation of absolute values of $\overline{\tilde{p}^2}$. However, a semi-empirical analysis of equation (7) can be performed in a manner analogous to that performed by Lighthill (ref. 8) for the case of acoustic power radiated from a region of turbulence. This should permit a determination of the shape of the fluctuation-pressure distribution along the jet. In Lighthill's case the entire turbulent region was characterized by a single characteristic velocity, frequency, and length. Moreover, the entire turbulent region contributed to pressure fluctuations at any given far-field observation point. In the present instance the situation is somewhat different, but analogous. Whereas in Lighthill's analysis a single value of a single quantity (total acoustic power) was sought, in the present instance a distribution of values of a single quantity (time-averaged pressure fluctuations) is sought. Thus, the entire turbulent region cannot be characterized by a single set of values of characteristic quantities. Rather, the characteristics of each region of the flow must be specified separately. Moreover, although the entire region of turbulence contributes to $\tilde{p}$ at any near-field observation point, the observed pressure fluctuations will be very strongly determined by turbulence in the flow immediately adjacent (see eq. (7) and ref. 7). This results because of the very rapid attenuation of $\overline{\tilde{p}^2}$ as a function of the source-point - observation-point separation $|\vec{y} - \vec{x}|$, or $|\vec{y} + \vec{z} - \vec{x}|$. Possibly the only related experimental data are presented in figure 16 of reference 4. These data show that for any given frequency the turbulence and pressure fluctuations peak at adjacent points along the jet

length. Thus, if it is assumed that the pressure fluctuations $\tilde{p}$ at a given observation point along the jet boundary are determined essentially by the turbulence within an adjacent limited volume τ of the jet, the analogy with Lighthill's analysis is complete.

Assume that the characteristic volume τ is proportional to an average eddy volume at the downstream location of the observation point. The eddy volume is approximately equal to the volume over which $\overline{\psi_{ij}(\vec{y};t)\psi_{kl}(\vec{y}+\vec{z};t)} \neq 0$, where $\vec{y}$ denotes a fixed point and $\vec{z}$ denotes a movable point. Let R represent a characteristic separation of the fixed point and the observation point; R corresponds to $|\vec{y} - \vec{x}|$ and $|\vec{y} + \vec{z} - \vec{x}|$ in equation (7). (For purposes of the analysis the effect of $\vec{z}$ on the values of other quantities may be disregarded, since only characteristic values are of interest.) Because the region influencing $\tilde{p}(\vec{x};t)$ extends only over the volume τ, it will be assumed that the integrations over $\vec{y}$ and $\vec{z}$ in equation (7) need only extend over τ, or possibly over a volume proportional to τ. The remaining factors $\frac{y_i - x_i}{|\vec{y} - \vec{x}|}$ and $\frac{y_i + z_i - x_i}{|\vec{y} + \vec{z} - \vec{x}|}$ represent directionality factors which are to be disregarded in an analysis of the present type.

The foregoing argument leads to the following expression for $\overline{\tilde{p}^2}$ along the jet boundary:

$$\overline{\tilde{p}^2} \propto \rho_0^2 \overline{\psi_{ij}\psi_{kl}} \tau^2 R^{-6}$$

It is usual to express the velocity components in a round jet in cylindrical (rather than rectangular Cartesian) coordinates r, φ, z. Let η_1, η_2, η_3 correspond to r, φ, z, respectively (see fig. 1). Let u_1, u_2, u_3 represent, respectively, the radial, azimuthal (dimensionless), and axial components of velocity in the cylindrical coordinate system. Velocity components in the two coordinate systems are typically related by

$$v_i = \frac{\partial y_i}{\partial \eta_k} u_k$$

where u, η in the cylindrical system correspond to v, y, respectively, in the rectangular system. The dimensional forms of the velocity components in the two coordinate systems differ only by trigonometric factors which are to be disregarded in the present analysis.

When $\overline{\psi_{ij}\psi_{kl}}$ is expanded in terms of the velocity components v_i (see eq. (3)), and hence u_i (see preceding paragraph), second-, third-,

and fourth-order covariances of the turbulent-velocity components result. The magnitudes of these covariances are generally not well known (ref. 5 and ref. 9, ch. VIII). However, because the mean-velocity component $\bar{u}_3$ is generally very much larger than any of the other components, the term $\psi_{3i} = \bar{u}_3\tilde{u}_i$, and hence the covariance $\overline{\psi_{3i}\psi_{3l}} = \bar{u}_3^2\,\overline{\tilde{u}_i\tilde{u}_l}$, should be expected to dominate. Thus, the dimensional representation of $\overline{\tilde{p}^2}$ may be rewritten as

$$\overline{\tilde{p}^2} \propto \rho_0^2\bar{u}_3^2\overline{\tilde{u}_i\tilde{u}_l}\tau^2R^{-6} \tag{8}$$

Proportionality (8) applies at any given point along the jet boundary. The variation of $\overline{\tilde{p}^2}$ as a function of ξ_3 is sought along the jet boundary, where ξ_3 is the jet axial coordinate of the observation point measured from the nozzle-exit plane. The situation is analogous to that of applying Lighthill's acoustic power relation (ref. 8) for similar jets. In addition to the usual requirements that the flows be geometrically similar and that the mean-flow and turbulent-flow Reynolds numbers be large, the present analysis implies that the eddies distributed along the jet be geometrically similar.

Along the jet, $\tau \propto \eta_3^3$ and $R \propto \eta_3$ (ref. 10). Hence,

$$\overline{\tilde{p}^2} \propto \rho_0^2\bar{u}_3^2\overline{\tilde{u}_i\tilde{u}_l} \tag{9}$$

For round subsonic jets where the mean-velocity distribution over the nozzle exit is uniform, similarity relations have been found (ref. 11, pp. 183-186) which relate velocity components $\bar{u}_i$, $\tilde{u}_i$ to the geometry of the jet. The relations and their associated regions of validity are as follows:

Region I: $1 \lessapprox \eta_3/d \lessapprox 4$

$$\bar{u}_3 = U_0F\left(\frac{\eta_3}{d}, \frac{\eta_1}{d}\right) \qquad \overline{\tilde{u}_3^2} = U_0^2G_{33}\left(\frac{\eta_3}{d}, \frac{\eta_1}{d}\right) \tag{10a}$$

Region II: $8 \lessapprox \eta_3/d \lessapprox 20$ to 50

$$\bar{u}_3 = U_0\,\frac{d}{\eta_3}\,f\left(\frac{\eta_1}{l}\right) \qquad \overline{\tilde{u}_\alpha\tilde{u}_\beta} = U_0^2G_{\alpha\beta}\left(\frac{\eta_3}{d}, \frac{\eta_1}{d}\right) \tag{10b}$$

Region III: $20 \text{ to } 50 \lessapprox \eta_3/d$

$$\overline{u}_3 = U_0 \frac{d}{\eta_3} f\left(\frac{\eta_1}{l}\right) \qquad \overline{\tilde{u}_\alpha \tilde{u}_\beta} = U_0^2 \frac{d^2}{\eta_3^2} g_{\alpha\beta}\left(\frac{\eta_1}{l}\right) \tag{10c}$$

where U_0 is exit velocity; d is nozzle-exit diameter; $l \propto \eta_3 - (\eta_3)_0$, where $(\eta_3)_0$ is the virtual origin of the jet; and $\alpha,\beta = 1,3$. Corresponding relations for the other components have not been determined. However, $\overline{u}_1 \ll \overline{u}_3$, and $\overline{u}_2 = 0$. The magnitudes of the unlisted turbulence covariances (containing the azimuthal components) are likely not greater than those given in equations (10).

In the notation of the preceding paragraph, region I is the mixing region. Region II is a region of self-preservation of the mean-velocity distribution. Region III is a region of self-preservation of the mean- and turbulent-velocity distributions called the region of fully developed turbulence.

The distribution of $\overline{\tilde{p}^2}$ as a function of η_3 is obtained by substituting the similarity relations (10) in proportionality (9). Thus,

Region I: $1 \lessapprox \eta_3/d \lessapprox 4$

$$\overline{\tilde{p}^2}/\left(\rho_0^2 U_0^4\right) \propto \left\langle F^2 G_{33} \right\rangle \tag{11a}$$

Region II: $8 \lessapprox \eta_3/d \lessapprox 20 \text{ to } 50$

$$\overline{\tilde{p}^2}/\left(\rho_0^2 U_0^4\right) \propto \left(\frac{d}{\eta_3}\right)^2 \left\langle f^2 G_{\alpha\beta} \right\rangle \tag{11b}$$

Region III: $20 \text{ to } 50 \lessapprox \eta_3/d$

$$\overline{\tilde{p}^2}/\left(\rho_0^2 U_0^4\right) \propto \left(\frac{d}{\eta_3}\right)^4 \left\langle f^2 g_{\alpha\beta} \right\rangle \tag{11c}$$

where $\langle\rangle$ denotes some form of space average over the volume τ.

Although F, G, f, and g are functions of η_3, the dependence is very weak compared with the dependence on η_1. The primary dependence of $\overline{\tilde{p}^2}$ on η_3 is contained in the coefficients of the velocity functions. Also, by virtue of the assumption that the observed pressure fluctuations at a given distance downstream of the nozzle exit are

determined by turbulence at the same distance downstream of the nozzle exit, the geometrical coordinate η_3 of the source point may be replaced by the coordinate ξ_3 denoting the observation point. It follows that, to a first approximation,

Region I: $1 \lessapprox \xi_3/d \lessapprox 4$

$$\overline{\tilde{p}^2}/\left(\rho_0^2 U_0^4\right) \propto (\xi_3/d)^0 \tag{12a}$$

Region II: $8 \lessapprox \xi_3/d \lessapprox 20 \text{ to } 50$

$$\overline{\tilde{p}^2}/\left(\rho_0^2 U_0^4\right) \propto (\xi_3/d)^{-2} \tag{12b}$$

Region III: $20 \text{ to } 50 \lessapprox \xi_3/d$

$$\overline{\tilde{p}^2}/\left(\rho_0^2 U_0^4\right) \propto (\xi_3/d)^{-4} \tag{12c}$$

Thus, the theoretical distribution of the time-averaged pressure fluctuations along the boundary of the mixing region ($1 \lessapprox \xi_3/d \lessapprox 4$) is flat, similar to that of the acoustic-source strength (ref. 1), that is, the power radiated per unit length of jet. However, along the boundary of the fully developed turbulent region ($20 \text{ to } 50 \lessapprox \xi_3/d$), the pressure fluctuations decay considerably less rapidly than does the acoustic-source strength, the decay law being proportional to ξ_3^{-4} for mean-square pressure and proportional to ξ_3^{-7} for source strength.

EXPERIMENT

Distributions of time-averaged fluctuating pressures along the mean-velocity boundary of round, cold, subsonic air jets were measured using 3- and 5-inch-diameter nozzles. Profiles of the nozzles are shown in figure 2. The measured pressure-fluctuation distributions are shown in figure 3. The distribution along a turbojet-engine exhaust (ref. 4) is also shown. The engine nozzle consisted of a straight tailpipe terminated by a spherical convergent iris. The engine exhaust pressure-fluctuation distribution is for a hot jet ($T \approx 1070^\circ$ F) at a slightly supercritical value of nozzle total-pressure ratio ($P/p_0 \approx 2.2$). A sound-level recorder possessing a quasi-peak averaging characteristic was used for the engine tests, whereas a meter having a full-wave rectified averaging characteristic was used for the air-jet tests.

The distributions in figure 3 have been replotted in the appropriate dimensionless form in figure 4. Corresponding theoretical curves are also shown. The distribution for the engine exhaust has been reduced by 3 decibels to account for the difference between the meter averaging characteristics. The shapes of the theoretical and experimental distributions tend to agree. However, the levels of the engine-exhaust and air-jet distributions differ, and the distribution for the 5-inch-diameter nozzle does not obey the $(\xi_3/d)^0$ law along the mixing region.

The level difference may result partly from inaccurate correction for the difference between the meter averaging characteristics and partly from dissimilarity of the microphone locations in the different tests. (Note that $\overline{\tilde{p}^2}$ is a strong function of ξ_1, near the nozzle (ref. 4).) However, dynamical and geometrical dissimilarity of the jets caused by the jet temperature difference and the nozzle-profile difference may have a greater influence on the level difference than the preceding factors. With regard to the effect of jet temperature, it should be noted that entropy fluctuations were neglected in the mathematical analysis and hence are neglected in the dimensionless ordinate used in figure 4. Also, jet temperature influences the space distribution of $\overline{\rho}$. The effect of jet temperature on the jet geometry is shown in reference 12. An increase in jet temperature tends to shorten the length of the jet core, increase the rate of jet spread, and increase turbulence levels. (In this connection, the microphone traverse angle with respect to the jet axis was the same (10°) in all tests.)

Some results are shown in figure 5 which illustrate the effect of different values of jet temperature on the fluctuation-pressure distribution. These tests were for the same nozzle (5-in. diam., fig. 2), so that nozzle geometry was not influential. The microphone traverse angle was also the same (11.5°) for all tests. Results are shown for a subcritical value of nozzle pressure ratio (fig. 5(a), $P/p_0 = 1.31$) and for a slightly supercritical value (fig. 5(b), $P/p_0 = 1.99$). As shown, for example by equations (12), the appropriate dimensionless ordinate for the subcritical-pressure-ratio case is $\overline{\tilde{p}^2}/\rho_0 U_0^2$. In the present instance (fig. 5(a)) this ordinate representation has been applied in the modified form

$$\Delta\left(20 \log \frac{\sqrt{\overline{\tilde{p}^2}}}{\rho_0 U_0^2}\right) = 20 \log \frac{\sqrt{\overline{\tilde{p}_2^2}}}{\left(\rho_0 U_0^2\right)_2} - 20 \log \frac{\sqrt{\overline{\tilde{p}_1^2}}}{\left(\rho_0 U_0^2\right)_1}$$

$$= SPL_2 - SPL_1 + 20 \log \frac{\left(\rho_0 U_0^2\right)_1}{\left(\rho_0 U_0^2\right)_2}$$

where SPL is sound pressure level (referred to 2×10^{-4} dyne/cm^2), the subscript 1 is associated with the lesser value of jet temperature, and the subscript 2 is associated with the greater value of jet temperature. By virtue of the representation $\sqrt{\overline{\tilde{p}^2}}/\rho_0 U_0^2$, the effect of the jet-velocity difference on pressure-fluctuation distributions measured for constant nozzle-pressure ratio should be eliminated. The representation $\sqrt{\overline{\tilde{p}^2}}/\rho_0 U_0^2$ is based on the assumption of incompressible flow. For supercritical values of pressure ratio the flow is certainly not incompressible. For nonisentropic jets operating at supercritical values of nozzle-pressure ratio, the pressure ratio I/p_0 has been found to be a correlating parameter for acoustic power generation at constant jet temperature (ref. 13). Applying this parameter in the present instance (fig. 5(b)), the appropriate ordinate representation for supercritical values of nozzle-pressure ratio is $\sqrt{\overline{\tilde{p}^2}}/P$, which in figure 5(b) has been applied in a modified form analogous to the subcritical ordinate representation.

The fluctuation-pressure levels plotted in figure 5 were repeatable within 1 decibel, except possibly for $\xi_3 > 50$ inches, where atmospheric winds were likely to influence the jet flow considerably. Although the temperature difference was small (82° F), the fluctuation pressures for the warmer jet were consistently higher near the nozzle than those for the cooler jet. Downstream of the nozzle, where jet temperatures tended to equalize, the pressure fluctuations (dimensionless form) tended to equalize. Thus, a definite effect of jet temperature on near-field pressure fluctuations is indicated.

The failure of the fluctuation-pressure distribution for the 5-inch-diameter nozzle to obey the $(\xi_3/d)^0$ decay relation illustrates the effect of the nozzle profile on the fluctuation-pressure distribution. It should be recalled that the velocity-similarity relations (10) apply only if the mean-velocity distribution over the nozzle exit is uniform. This condition is certainly not satisfied in the case of the 5-inch-diameter nozzle. Schlieren photographs of the flow from the 5-inch-diameter nozzle have shown the emergent boundary layer to be highly turbulent. In contrast, schlieren photographs of the flow from the 3-inch-diameter nozzle have shown the emergent boundary layer to be quasi-laminar downstream to a vena contracta, from which plane the jet expands and the mixing region becomes highly turbulent. In this case the mean-velocity distribution over the nozzle exit can be expected to be fairly uniform. The convergence of the nozzle produces a negative pressure gradient which tends to preserve laminar flow in the boundary layer. Sketches of the expected flows from the two nozzles are shown in figure 6. On the dimensionless basis $\left(\sqrt{\overline{\tilde{p}^2}}/\rho_0 U_0^2\right)$, pressure fluctuations of larger magnitude

should be expected near the exit of the 5-inch-diameter nozzle. Also, the ratio of the maximum averaged fluctuation pressure to the value of the averaged fluctuation pressure at the nozzle-exit plane should be expected to be greater for the 3-inch-diameter nozzle by virtue of the fact that the emergent boundary layer has transformed from quasi laminar to turbulent. These expectations are confirmed in figure 4. The effect of dissimilarity of the nozzle profiles on near-field pressure fluctuations is considerable.

CONCLUSIONS

The incompressible-fluid theory for near-field pressure fluctuations in conjunction with jet similarity relations appears to account for the general shape of the distribution of time-averaged pressure fluctuations along the mean-velocity boundary of a round subsonic jet with uniform exit velocity. However, jet temperature, which is not considered in the theory, significantly affects the values of the fluctuations and the fluctuation distribution, especially near the nozzle. Higher jet temperatures result in larger pressure fluctuations. The jet-nozzle profile can also significantly affect the fluctuation-pressure distribution, especially near the nozzle, by introducing a nonuniform exit-velocity distribution.

Lewis Research Center
National Aeronautics and Space Administration
Cleveland, Ohio, July 22, 1960

APPENDIX - SYMBOLS

d	jet-nozzle-exit diameter
$d^3\vec{y}, d^3\vec{y}', d^3\vec{z}$	volume elements
F,G	velocity distribution functions
f,g	self-preserving velocity distribution functions
P	stagnation pressure
p	static pressure
p_0	ambient pressure
R	characteristic separation of source point and observation point
T	temperature
t	time
U_0	jet-exit (core) velocity
u_i	velocity components in cylindrical coordinate system
v_i	velocity components in rectangular Cartesian coordinate system
x_i	rectangular Cartesian coordinates of observation point (origin at center of nozzle exit; see fig. 1)
y_i	rectangular Cartesian coordinates of source point (origin at center of nozzle exit; see fig. 1)
z_i	rectangular Cartesian coordinates of source point (origin at another source point)
η_i	cylindrical coordinates of source point (origin at center of nozzle exit; see fig. 1)
ξ_i	cylindrical coordinates of observation point (origin at center of nozzle exit; see fig. 1)
ρ	density
ρ_0	ambient density

τ	characteristic local eddy volume
ψ_{ij}	$2\overline{v}_i\tilde{v}_j + \tilde{v}_i\tilde{v}_j - \overline{\tilde{v}_i\tilde{v}_j}$
$\langle\rangle$	space average over volume τ

Subscripts:

$\alpha,\beta = 1,3$	components in cylindrical coordinate system (1, radial component; 3, jet axial component)
$i,j,k,l = 1,2,3$	components in coordinate systems (In rectangular Cartesian coordinates: 1,2, components normal to jet axis; 3, jet axial component. In cylindrical coordinates: 1, radial component; 2, azimuthal component, 3, jet axial component.)

Superscripts:

$\overline{\quad}$	time average
$\sim$	incompressible fluctuation
$'$	source point or observation point generally different than that associated with corresponding unprimed quantity
$\rightarrow$	vector

E-780

REFERENCES

1. Ribner, H. S.: On the Strength Distribution of Noise Sources Along a Jet. Rep. 51, Inst. Aerophys., Univ. Toronto, Apr. 1958. (See also Jour. Acoustical Soc. Am., vol. 30, 1958, p. 876.)

2. Powell, Alan: Similarity Considerations of Noise Production from Turbulent Jets, Both Static and Moving. Rep. SM-23246, Douglas Aircraft Co., Inc., July 1, 1958.

3. Lilley, G. M.: On the Noise from Air Jets. FM 2724, British ARC, Sept. 8. 1958.

4. Howes, Walton L., Callaghan, Edmund E., Coles, Willard D., and Mull, Harold R.: Near Noise Field of a Jet-Engine Exhaust. NACA Rep. 1338, 1957. (Supersedes NACA TN's 3763 and 3764.)

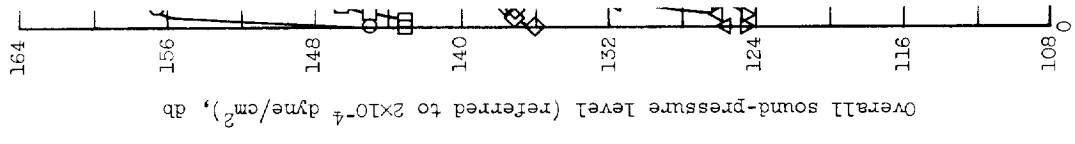

16

18

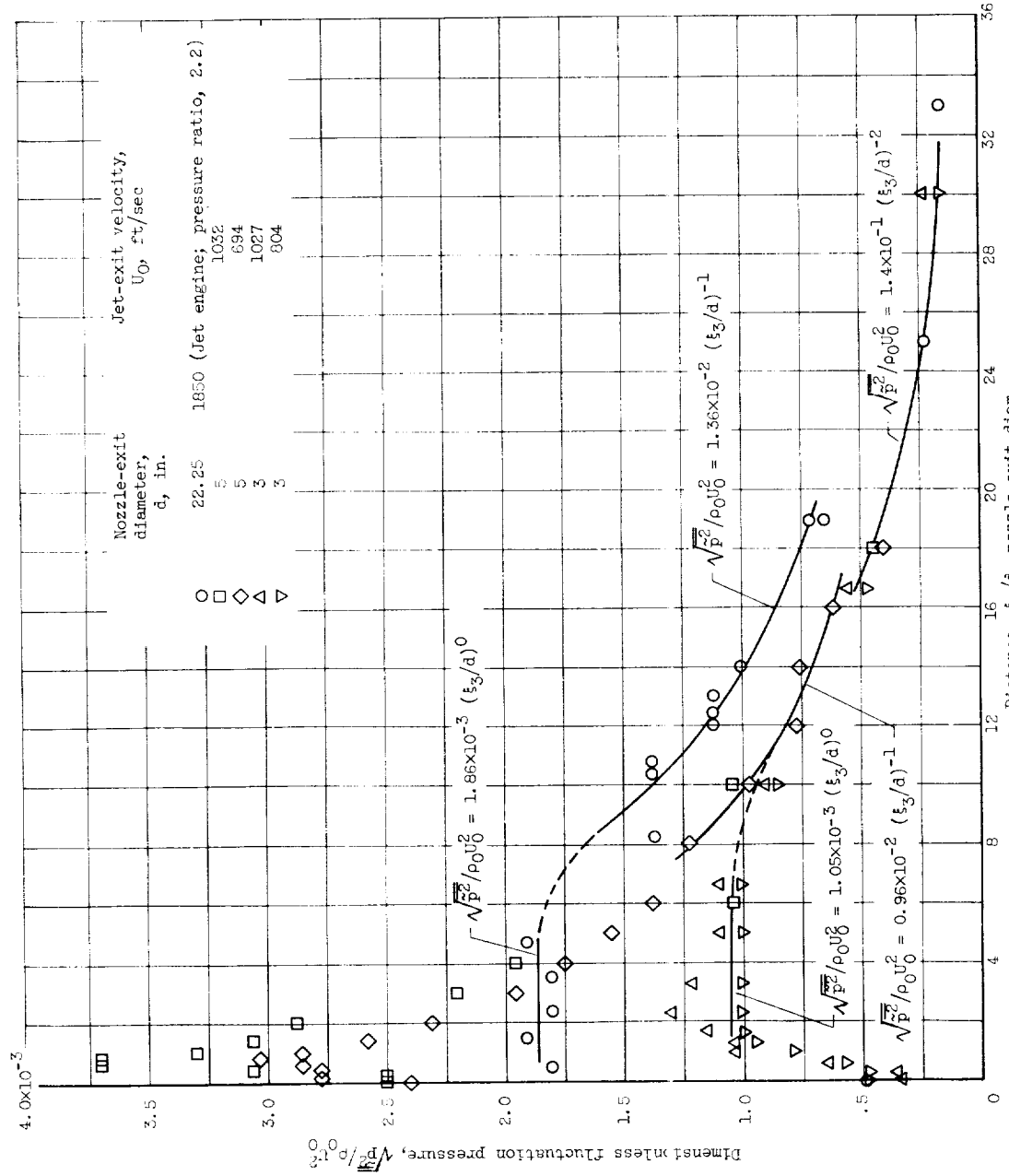

Figure 4. - Dimensionless fluctuation-pressure distributions along mean-velocity boundary.

E-780

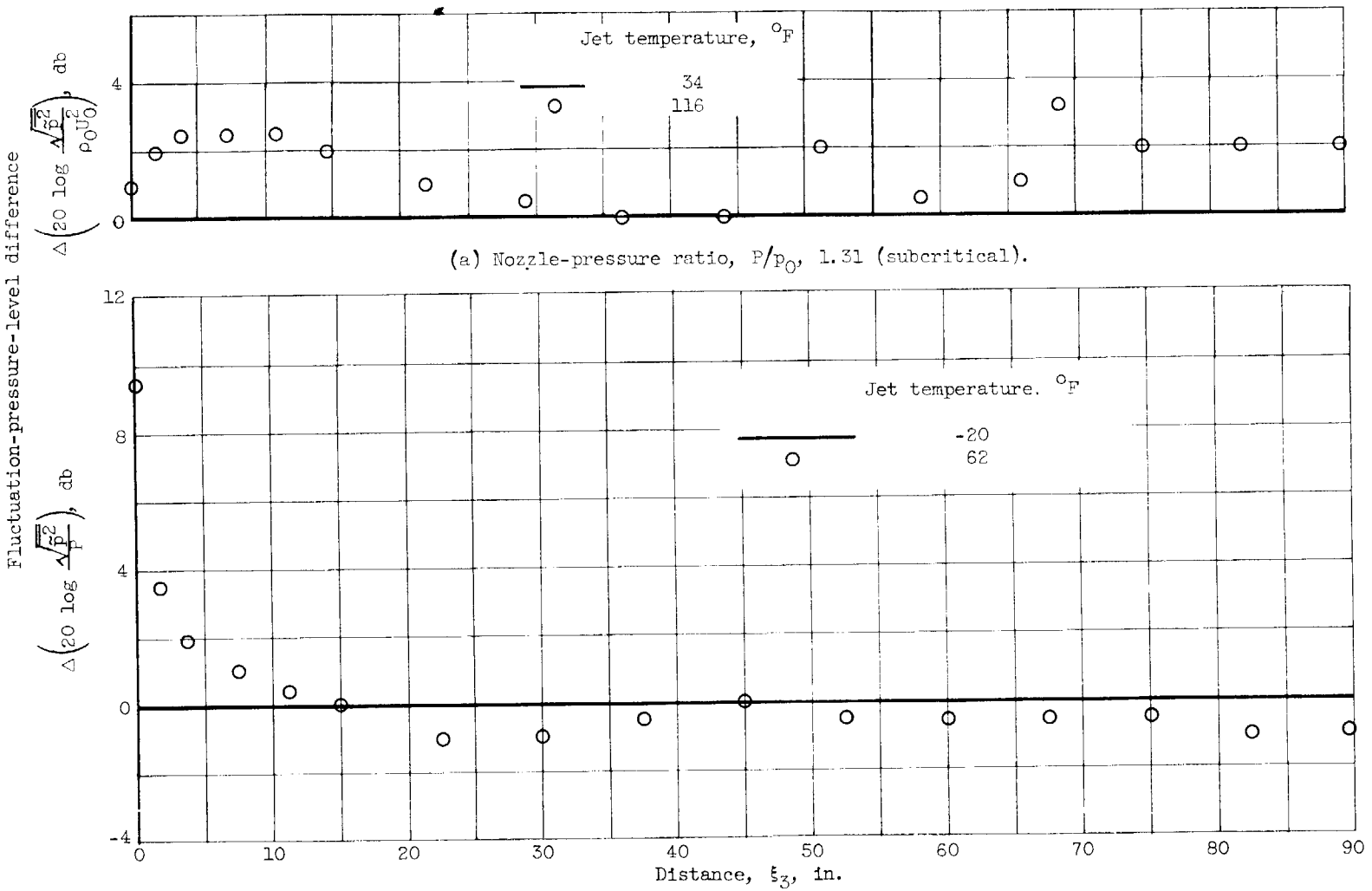

Figure 5. - Effect of jet temperature on fluctuation-pressure distribution along mean-velocity boundary. Nozzle-exit diameter, 5 inches; ambient temperature, 71° F.

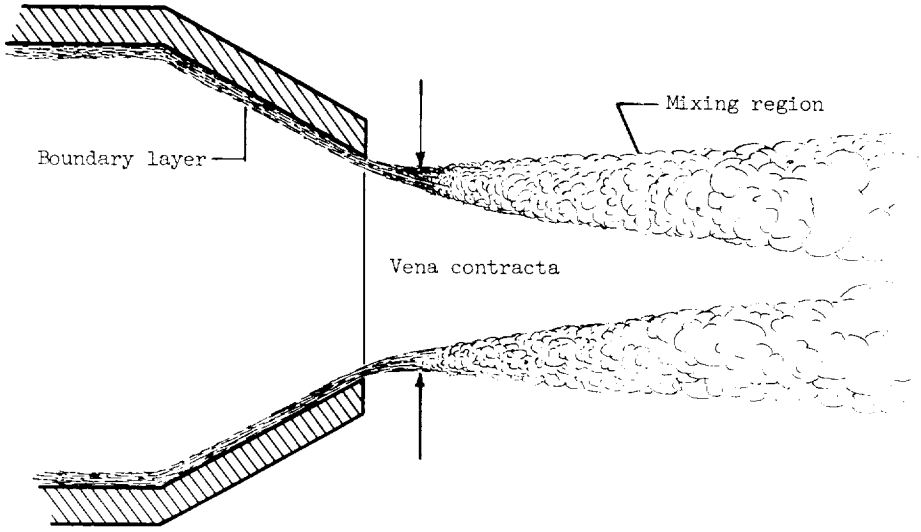

(a) 3-inch-diameter nozzle.

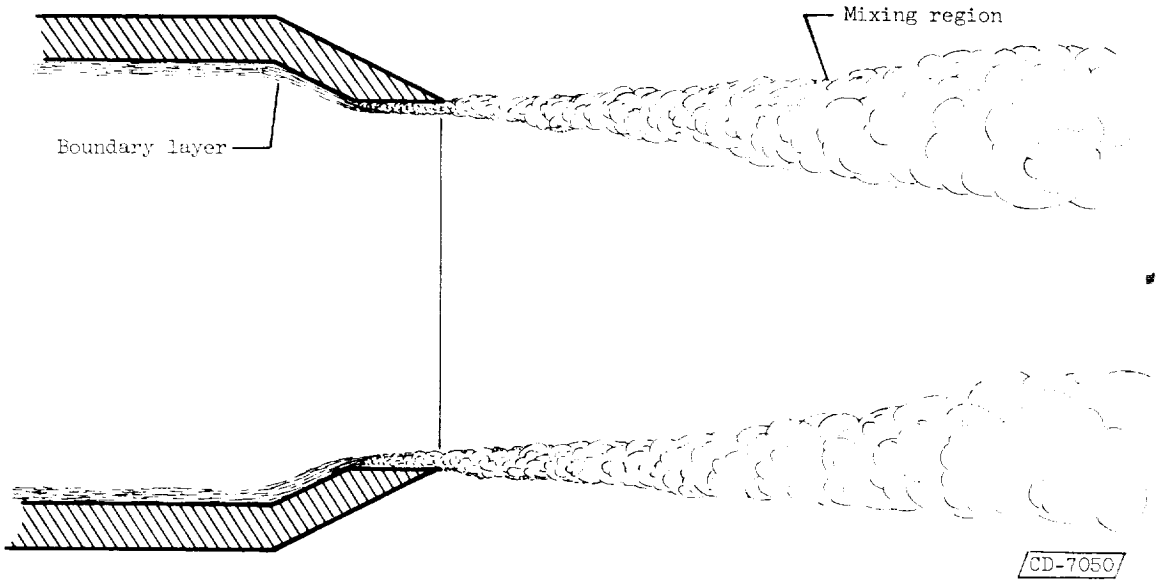

(b) 5-inch-diameter nozzle.

Figure 6. - Expected flow patterns from test nozzles.